Vehicle agile maneuvering: From rally drivers to a finite state machine approach

Manuel Acosta
School of Mechanical, Aerospace and Automotive Engineering
Coventry University
United Kingdom
ac3354@coventry.ac.uk

Stratis Kanarachos
School of Mechanical, Aerospace and Automotive Engineering
Coventry University
United Kingdom
ab8522@coventry.ac.uk

Mike Blundell
School of Mechanical, Aerospace and Automotive Engineering
Coventry University
United Kingdom
cex403@coventry.ac.uk

***Abstract*- Rally drivers can perform extreme maneuvers and keep a vehicle on track by maximizing the vehicle agility. It is remarkable that this is achieved robustly, without a vehicle or tire model in mind. In this study, the Moment Method Diagram and Beta Method representations are used to show the maximum achievable yaw moment generated by the front and rear tires. A new maneuverability map is proposed to bypass the limitations imposed by the steady-state assumptions, based on the wheel slip – yaw moment representation. Furthermore, a simple driving automation strategy is developed to determine the sequence of inputs required for maximizing vehicle agility and negotiating extreme maneuvers. A finite state machine is designed and implemented using a two track vehicle model. The numerical results show that the finite state machine can resemble a rally driver.**

Keywords—agile maneuvering; autonomous driving; finite state machine; drift

I. INTRODUCTION

Agile maneuvering is conceived as the ability of the driver-vehicle interaction to generate important changes in vehicle attitude in a reduced amount of time. Normally, regular drivers approach corners in quasi-steady-state conditions [1], that is, with reduced yaw acceleration. Nevertheless, rally drivers are able to achieve high values of yaw acceleration to make fast transitions through reduced radius turns, e.g. Hairpin turns, thus using the full agility potential of the vehicle [2]. Due to the growing interest of the automotive industry in designing intelligent systems capable of operating autonomously and safely beyond the linear region limits, it is of vital important to understand how high yaw moments can be achieved [3,4].

In this paper, relevant background in agile maneuvering is presented. The most extended representations of vehicle handling dynamics (Milliken Moment Method *MMD* [1] and Beta Method [5, 6]) are described to understand the full agility potential of the car and how to exploit it. Additionally, a new portrait (wheel slip – yaw Moment) is used to determine the combination of front and rear wheel slips required to generate a target yaw moment. Then, a finite state machine *FSM* is implemented in a two track vehicle model (*Matlab*® / *Simulink*®). The *FSM* computes (based on the chassis agility potential) the inputs required to achieve a target yaw moment. Furthermore, in addition to the simulation results, metrics to characterize the vehicle agility are proposed (attitude change time (t_ψ), min sideslip (β), min sideslip rate ($\dot{\beta}$) and max. yaw acceleration ($\dot{r}$)). Conclusions and further steps are presented in the last section.

II. BACKGROUND

A. Agile maneuvering

Different approaches have been used to analyze agile maneuvering. Velenis, Tsiotras, Lu [7] studied the maneuvers commonly performed by Rally drivers (Trail braking and Pendulum turn) from an optimization perspective. Olofsson, Lundhal, Berntorp, Nielsen, [8] found that in order to minimize the time to negotiate a Hairpin turn, it is necessary to generate high sideslip angles (up to 40 deg). An important conclusion extracted from these works is that although the vehicle attitude is strongly dependent on the road grip, the vehicle trajectory remains almost invariant. This could benefit potential applications of path following strategies in agile autonomous vehicles if the heading information is known in advance.

On the other hand, other authors have focused on analyzing the vehicle stability and controllability when operating with high sideslip angles (Drift equilibrium). Edelmann, Ploch [9] used the root locus portrait to demonstrate that the drifting dynamics are highly unstable. Velenis, Katzourakis, Frazzoli, Tsiotras, Happee [10] implemented an LQR to stabilize the vehicle around a high sideslip solution (drift control) and compare the results obtained from numerical simulations and experimental data. Finally, Li, Zhang, Yi, Liu [11] studied the

limits of the stable (yaw rate - rear wheel slip) phase portrait for different steering values. They proposed an extension of the boundaries of the "stable area" under the term "safety boundary", in which highly skilled drivers are able to operate and the full chassis potential is used.

B. Moment Method Diagram

The *MMD*, *"Fig. 1"*, first appeared in the Milliken publication (Race Car Vehicle Dynamics [1]). It represents the lateral acceleration versus the normalized yaw moment (1) for different combinations of sideslip and steering angle.

$$C_N = \frac{N}{mg(l_f + l_r)} \tag{1}$$

The diagram is constructed by solving the planar dynamic equations for a given constant speed and assuming steady-state conditions (null sideslip rate). Overall, it provides valuable information regarding chassis performance: grip limit, directional stability and maximum achievable yaw moment. A detailed description of this diagram as well as a study of the influence of different setup changes on the *MMD* shape is presented in [1]. Additionally, other works [12, 13] have used this representation intensively to evaluate vehicle stability and controllability.

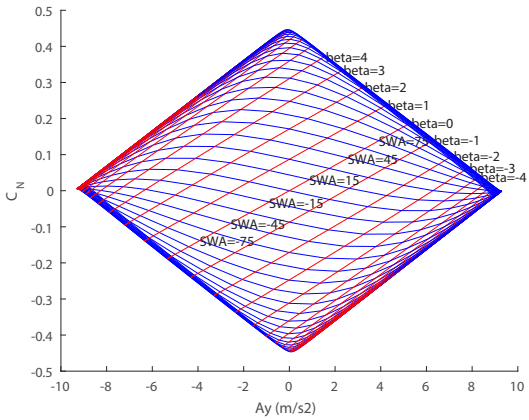

Fig. 1. *MMD* generated in *Matlab*® with the parameters showed in "*Table I.*" at 80 kph.

The *MMD* presented above was generated using the vehicle parameters detailed in Table I. The ISO sign convention was followed in this paper and the tire model is described in Section III. In this case, the vehicle exhibits a slight understeer tendency at the limit (recovering yaw moment) and a maximum lateral acceleration of 9.2 m/s2 approximately. The symbols used in this paper can be consulted in the last Section, Nomenclature.

TABLE I. Vehicle parameters

Notation	Value	Unit	Notation	Value	Unit
l_f	1.25	$[m]$	I_z	2500	$[kgm^2]$
l_r	1.35	$[m]$	$k_{\varphi f}$	110000	$[Nm/rad]$
m	1500	$[kg]$	$k_{\varphi r}$	70000	$[Nm/rad]$
t_{wf}	1.5	$[m]$	h_{CoG}	0.5	$[m]$
t_{wr}	1.5	$[m]$	SR	15	[-]

The influence of the speed in the directional stability of the vehicle is observed in *"Fig. 2.a"* and *"Fig. 2.b"*. At moderate speeds (left), the slope of the constant steer angle lines is very pronounced, and any lateral perturbation will be counteracted by a stabilizing yaw moment. Conversely, at high speeds (right), the slope reduces considerably and little stabilizing moment is expected under lateral perturbations. It is important to remark that the contribution of the downforce is neglected in this analysis (passenger car). Therefore, the envelope of the diagram is expected to maintain constant regardless of the speed.

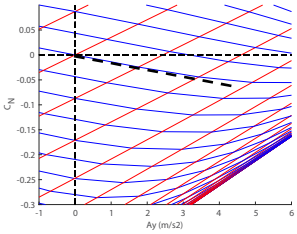

Fig. 2. a. Detail of the *MMD* at 80 kph.

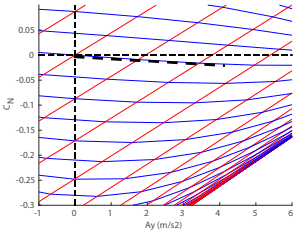

Fig. 2. b. Detail of the *MMD* at 140 kph.

Finally, the diagram can be used to predict the vehicle states in a steady-state maneuver. Thus, standard representations such as *sideslip – Ay* or *steering angle – Ay*, often used in chassis evaluation, can be obtained for constant speed tests. E.g. "Slow increasing steer test" [1].

C. Beta Method diagram

The beta-method was developed by Shibahata, Shimada, Tomari [6] to study the influence of the sideslip angle on the vehicle controllability. This representation contains the same basic information as the *MMD*, but in this case, the sideslip angle is plotted on the horizontal axis. These axes facilitate the study of the relation between the sideslip and the remaining controllability (yaw moment) that can be used by the driver.

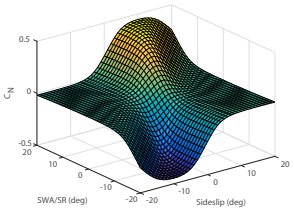

Fig. 3. a. 3D representation of the Beta diagram.

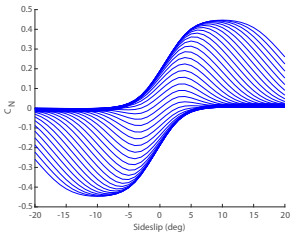

Fig. 3. b. 2D projection of the Beta diagram on the $C_N - \beta$ plane.

"Fig. 3.a" depicts the Beta Method surface generated from the *MMD*. The normalized yaw moment (C_N) is plotted for each (δ, β) data pair (left). The surface is then projected on the $C_N - \beta$ plane, obtaining the Beta Method diagram. Each line represents a constant steering wheel angle. As pointed out by A. Zanten [5], the yaw moment available decreases dramatically when the sideslip angle passes a certain threshold. This is noticed in *"Fig. 3.b"*. If the sideslip angle is augmented while the steering angle is maintained (moving in the constant steering angle lines), the yaw moment reaches peak values between 5-10 degrees, and then diminishes abruptly. It is important to notice that the maximum yaw moment is achieved

for combinations of steering and sideslip angle. To conclude, it can be understood from the work presented in this section that the yaw moment generated by the car will depend on the (δ, β) pair. In other words, the yaw moment with which the vehicle will start a maneuver from steady-state conditions can be predicted if δ and β are known.

III. Description of the Vehicle Model

In this paper, a simplified two track model was constructed in (*Matlab® / Simulink®*) to evaluate the vehicle responses under different inputs. This section describes the planar dynamics, lateral and longitudinal weight transfer and tire model equations used in the model. The numerical values of the vehicle parameters were listed in the previous section ("Table I").

A. Planar dynamics

The vehicle planar dynamics *("Fig 4")* were modeled assuming negligible influence of the pitch and roll dynamics on the yaw motion (2-4):

$$(F_{x,1}+F_{x,2})\cos(\delta)-(F_{y,1}+F_{y,2})\sin(\delta)+F_{x,3}+F_{x,4}=m(\dot{v}_x-v_y r) \quad (2)$$

$$(F_{y,1}+F_{y,2})\cos(\delta)+(F_{x,1}+F_{x,2})\sin(\delta)+F_{y,3}+F_{y,4}=m(\dot{v}_y+v_x r) \quad (3)$$

$$(F_{y,1}+F_{y,2})\cos(\delta)\,l_f+(F_{x,1}+F_{x,2})\sin(\delta)\,l_f-(F_{y,3}+F_{y,4})l_r+\frac{t_{wf}}{2}(F_{x,2}-F_{x,1})\cos(\delta)+\frac{t_{wf}}{2}(F_{y,1}-F_{y,2})\sin(\delta)+\frac{t_{wr}}{2}(F_{x,4}-F_{x,3})=I_z\dot{r} \quad (4)$$

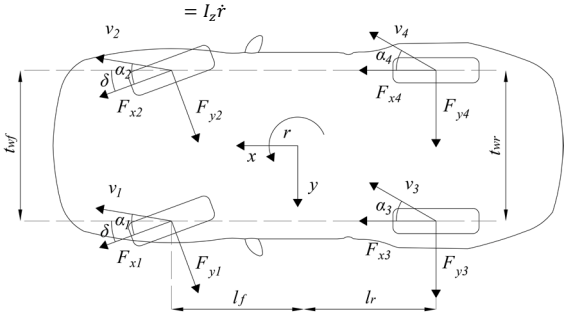

Fig. 4. Scheme of the planar dynamics model.

B. Kinematic equations

Wheel slips are calculated according to the following kinematic expressions (5-8):

$$\alpha_1=\delta-\arctan\left(\frac{rl_f+v_y}{v_x-\frac{rt_{wf}}{2}}\right) \quad (5)$$

$$\alpha_2=\delta-\arctan\left(\frac{rl_f+v_y}{v_x+\frac{rt_{wf}}{2}}\right) \quad (6)$$

$$\alpha_3=-\arctan\left(\frac{-rl_r+v_y}{v_x-\frac{rt_{wr}}{2}}\right) \quad (7)$$

$$\alpha_4=-\arctan\left(\frac{-rl_r+v_y}{v_x+\frac{rt_{wr}}{2}}\right) \quad (8)$$

In this paper, changes in wheel slip due to suspension compliances are not considered. In addition, expressions (5-8) can be simplified into (9-10) if the small angles assumption $\sin(\theta)\approx\theta$ is taken and the term $\left(\frac{rt_w}{2}\right)$ is neglected.

$$\alpha_f=\delta-\left(\frac{rl_f}{v_x}+\frac{v_y}{v_x}\right) \quad (9)$$

$$\alpha_r=-\left(-\frac{rl_r}{v_x}+\frac{v_y}{v_x}\right) \quad (10)$$

C. Weight transfer

Vertical loads are calculated considering quasi-static longitudinal and lateral weight transfer (11-13). For simplicity, only weight transfer through springs is taken into account (dampers are not modeled). Additionally, the roll center is considered to lie on the ground.

$$F_{z,i}=\frac{mgl_j}{2WB}\mp\Delta F_{z,long}\mp\Delta F_{z,latj}\;\; i\in\{1,2,3,4\}, j\in\{f,r\} \quad (11)$$

$$\Delta F_{z,long}=\frac{mh_{CoG}}{2WB}a_x \quad (12)$$

$$\Delta F_{z,latj}=\frac{mh_{CoG}}{t_{wj}}\left(\frac{k_{\varphi j}}{k_{\varphi f}+k_{\varphi r}}\right)a_y,\qquad j\in\{f,r\} \quad (13)$$

D. Tire model

Tires are modeled using an empirical model, *Magic Formula*. Equations (14-15) [8] are used to compute the pure longitudinal and lateral forces. A weighting factor (16-21) is then applied to capture the effects of the interaction between longitudinal and lateral slips *("Fig 5")*.

$$\mathrm{F_{x0,i}}=\mu_{x,i}F_{z,i}\sin\left(C_{x,i}\,arctan\left(B_{x,i}\lambda_i-E_{x,i}\left(B_{x,i}\lambda_i-arctan\left(B_{x,i}\lambda_i\right)\right)\right)\right) \quad (14)$$

$$\mathrm{F_{y0,i}}=\mu_{y,i}F_{z,i}\sin\left(C_{y,i}\,arctan\left(B_{y,i}\alpha_i-E_{y,i}\left(B_{y,i}\alpha_i-arctan\left(B_{y,i}\alpha_i\right)\right)\right)\right) \quad (15)$$

$$H_{x\alpha,i}=B_{x1,i}\cos\left(arctan\left(B_{x2,i}\lambda_i\right)\right) \quad (16)$$

$$G_{x\alpha,i}=\cos\left(C_{x\alpha,i}\arctan\left(H_{x\alpha,i}\alpha_i\right)\right) \quad (17)$$

$$H_{y\lambda,i}=B_{y1,i}\cos\left(arctan\left(B_{y2,i}\alpha_i\right)\right) \quad (18)$$

$$G_{y\lambda,i}=\cos\left(C_{y\lambda,i}\arctan\left(H_{y\lambda,i}\lambda_i\right)\right) \quad (19)$$

$$F_{x,i}=F_{x0,i}G_{x\alpha,i},\qquad i\in\{1,2,3,4\}, \quad (20)$$

$$F_{y,i}=F_{y0,i}G_{y\lambda,i},\qquad i\in\{1,2,3,4\}, \quad (21)$$

The tire parameters used in this work are listed in Table II, and were extracted from [8].

TABLE II. Tire model parameters

Notation	Front	Rear	Notation	Front	Rear
μ_x	1.2	1.2	μ_y	0.935	0.961
C_x	1.69	1.69	C_y	1.19	1.19
B_x	11.7	11.1	B_y	8.86	9.3
E_x	0.377	0.362	E_y	-1.21	-1.11
B_{x1}	12.4	12.4	B_{y1}	6.46	6.46
B_{x2}	-10.8	-10.8	B_{y2}	4.20	4.20
$C_{x\alpha}$	1.09	1.09	$C_{y\lambda}$	1.08	1.08

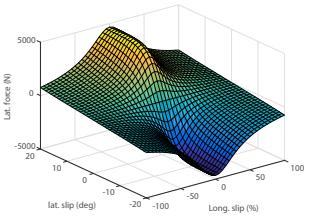

Fig. 5. a. Combined lateral force surface.

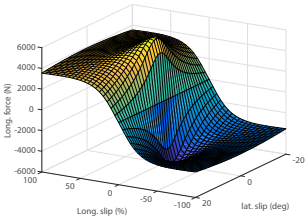

Fig. 5. b. Combined longitudinal force surface.

IV. GENERATING MAXIMUM YAW MOMENT

In Section II the *MMD* and Beta Method representations were presented. As will be explained in this section, these diagrams are fundamental to understand how the full agility of the vehicle can be exploited. *"Fig. 6"* illustrates two snapshots of a vehicle driving in a straight line. In *"Fig 6.a"*, the vehicle sideslip is zero, being the velocity vector perfectly aligned with the tangent of the path. On the other hand, *"Fig 6.b"* shows a vehicle in which a positive sideslip angle has been induced.

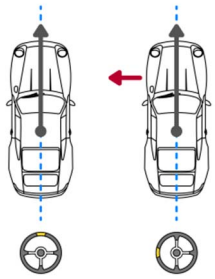

Fig. 6. a. Normal step input.

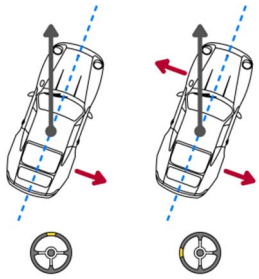

Fig. 6. b. Step input with sideslip angle.

For simplicity, restrictions in the maximum steering wheel velocity are not considered, and a sudden steering input (δ) is applied to negotiate a sharp left-handed turn. Assuming that the steering input is fast enough (step shape), the yaw moment generated at each situation can be evaluated in the *MMD*, *"Fig. 7"*.

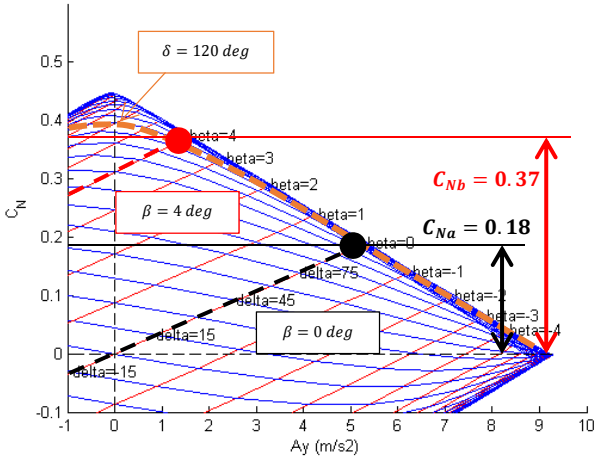

Fig. 7. Situations 6.a and 6.b illustrated in the *MMD*. Note the difference in yaw moment depending on the initial sideslip angle

As can be clearly appreciated in *"Fig. 7"*, the yaw moment generated in situation *"b"*, C_{Nb} is considerably higher than the yaw moment created in situation *"a"*, C_{Na}. Evaluating the *MMD* and *Beta-Method* representations *("Fig. 8")*, the high agility regions (max. yaw moment) can be achieved only for combinations of sideslip and steering inputs. The physical explanation of this phenomenon resides on the tire lateral forces and the delay between them.

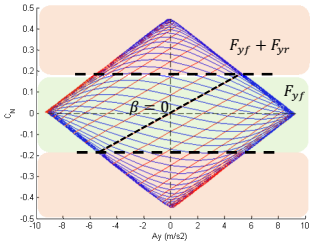

Fig. 8. a. *MMD*, regions of maximum yaw moment.

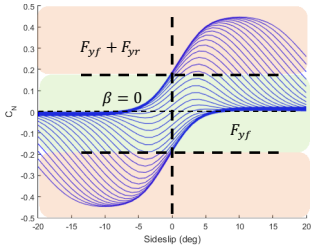

Fig. 8. b. Beta diagram, regions of maximum yaw moment.

In situation *"b"*, the front and rear tire lateral forces are out-of-phase and both contribute to create a yaw moment around the center of gravity. Thus, while the maximum yaw moment in situation *"a"* is limited by the front tire forces, the maximum yaw moment of situation *"b"* is created by both front and rear tires. *"Fig. 8 a"* and *"Fig. 8 b"* illustrate the limits of achievable yaw moment by the front tires (green shaded area) for null sideslip angle. This combination of sideslip angle with an adequate steering input is habitual in motorsport, e.g. Rally driving, when skilled drivers execute the Scandinavian Flick to change quickly the vehicle attitude in low grip conditions, trying to reduce the understeer of the vehicle. The same phenomenon is observed when the chassis is subjected to high-frequency steering inputs, i.e. in a frequency response tests. When the steering frequency approaches the minimum acceleration gain region (1-2 Hz), the delay between the front and rear wheel slips is high and the axle lateral forces can be out-of-phase.

A. *Limitations of the MMD (sideslip rate)*

From the previous sections, it is clear that there exist certain combinations of β and δ that permit achieving high yaw moments (high agility regions). Therefore, one might think that a suitable approach to reach these regions could be to use the diagrams presented. Nevertheless, it must be mentioned that these representations are generated under the assumption of steady-state conditions (or in other words, considering null sideslip rate).

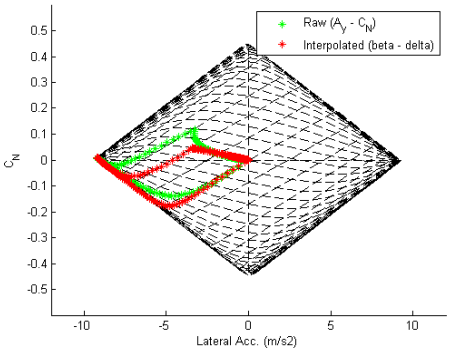

Fig. 9. Raw data from simulation ($C_N - A_y$) and interpolated trajectories ($\beta - \delta$) on the *MMD*.

In *"Fig. 9"*, two trajectories are plotted in the *MMD*. Both trajectories correspond to the same maneuver (Simulated Sine with Dwell), however, the green trace is formed by ($A_y - C_N$)

coordinates while the red one contains interpolated $(\beta - \delta)$ points. The trajectories differ considerably in the diagram due to the high transient content of the maneuver. For this reason, if the yaw moment is to be predicted from the vehicle states an alternative representation is necessary.

B. *Maneuverability map*

In this paper, the wheel slip versus yaw moment diagram is proposed as a robust maneuverability map. According to (4), under the assumption of small angles and neglecting the contribution of longitudinal forces, the yaw moment depends only on the axle lateral forces. These last are a function of the longitudinal wheel slips, vertical forces and lateral wheel slips (9-10). Therefore, for each combination of (α_f, α_r) there exist a yaw moment, regardless of the sideslip rate. *"Fig. 10"* shows schematically the construction of the maneuverability map.

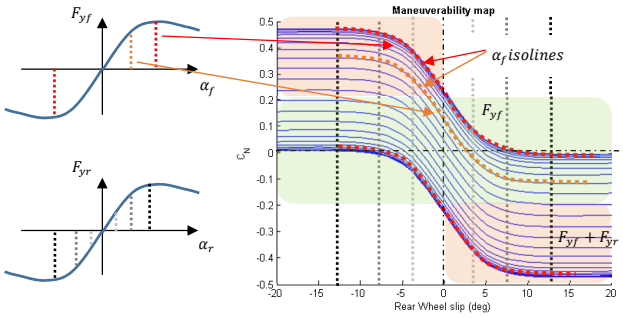

Fig. 10. Construction of the maneuverability map.

"Fig.11 a" and *"Fig.11 b"* represent the diagram for different values of longitudinal and lateral acceleration. No influence of the lateral weight transfer is expected from the tire model used (lateral – vertical force proportionality, (14-15)).

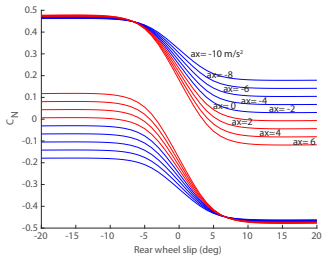

Fig. 11. a. Influence of long. Weight transfer.

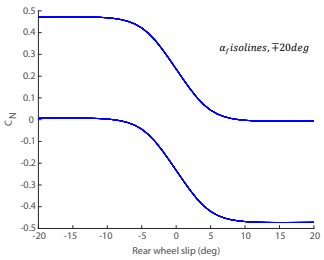

Fig. 11. b. Influence of lat. Weight transfer.

"Fig. 12 a" and *"Fig. 12 b"* depict the maneuverability map for different values of front and rear longitudinal slip. Expectedly, both front and rear longitudinal slips reduce the maximum achievable yaw moment due to the reduction of the available lateral forces. Finally, the road grip "scales" the map, reducing the total controllability area in low grip situations.

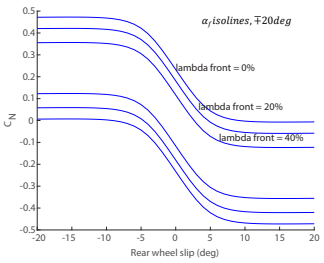

Fig. 12. a. Influence of front long. slip.

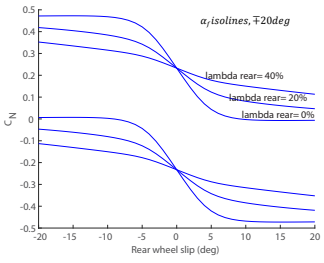

Fig. 12. b. Influence of rear long. slip.

Although the longitudinal slip and longitudinal weight transfer are coupled, they have been analyzed individually with the objective to facilitate the evaluation of each factor on the maneuverability map. The principle of superposition could be applied to study the total contribution of these factors on the map.

V. FINITE STATE MACHINE

A. *Description of the Finite State Machine*

The *FSM* proposed in this paper consists of three states *("Fig. 13")*. State 1 corresponds to the vehicle driving in a straight line at constant speed, before starting the maneuver. When a target yaw moment (M_{zref}) is given to the machine, the current state can change to State 2 or State 3.

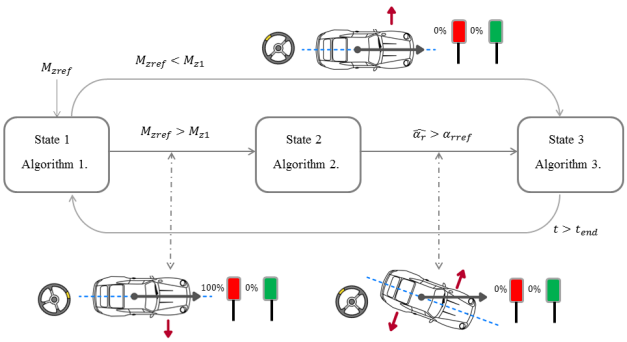

Fig. 13. State diagram of the Finite State Machine.

If M_{zref} is higher than the threshold M_{z1}, the machine switchs to State 2. If not, the machine goes directly to State 3. In State 2, the machine applies the steering and braking actions required to reach the rear wheel slip condition (α_{rref}) necessary to achieve M_{zref}. Finally, when the wheel slip condition is satisfactory, the machine switches to State 3, and the second steering input is applied to generate M_{zref}.

B. *State 1 (Yaw moment Threshold)*

The moment threshold M_{z1} is equal to the maximum yaw moment that can be generated only with the front tires ($\approx F_{yf} l_f$). The reference moment is evaluated in the Algorithm 1, expressed as follows:

Algorithm 1 Reference yaw moment evaluation

Input: Reference yaw moment (M_{zref})

Output: System State, vehicle inputs ($\delta, \lambda_f, \lambda_r$), target rear slip ($\alpha_{rref}$)

1: If $abs(M_{zref})<M_{z1}$

2: $\alpha_{rref} = 0, \delta = SR \cdot \alpha_{fref}$,$\lambda_f = 0, \lambda_r = 0$,

3: State=State 3

4: Else

5: $\alpha_r = \alpha_{rref}, \delta = -\delta_1 \cdot sign(M_{zref}), \lambda_f = 0, \lambda_r = -1$,

6: State=State 2

7: end

Where the wheel slips ($\alpha_{rref}, \alpha_{fref}$) are calculated from the maneuverability map *"Fig. 15. a"*. The amplitude of the steering input δ_1 is calculated by linear interpolation of the values showed in the look-up table, Table III.

TABLE III. First input (δ_1) look-up table

v_x (kph)	$\alpha_{rref} = 5\ deg$	$\alpha_{rref} = 10\ deg$	$\alpha_{rref} = 15\ deg$
60	60	70	75
80	55	60	65
100	50	55	60
120	50	55	55

The look-up table is generated by simulation. The rear wheels are locked ($\lambda_r = -1$) and steering steps of increasing amplitudes are applied at different speeds. The time to reach different target rear wheel slips (t_{5r}, t_{10r}, t_{15r}) is saved. As can be observed in the surface of *"Fig.14 a"*, the time required to achieve a rear wheel slip value of ten degrees, t_{10r}, decreases considerably with the steering amplitude. *"Fig 14. b"* shows t_{5r} for different rear longitudinal slips. Expectedly, the time is minimized when the rear wheels are fully locked, which justifies the $\lambda_r = -1$ condition.

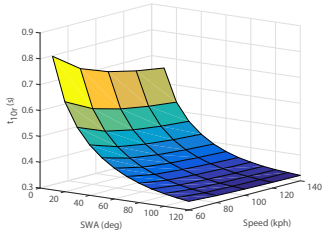

Fig. 14. a. Response time surface,$\alpha_{rref} = 10$ degrees.

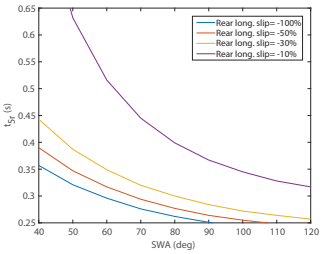

Fig. 14. b. Response time for different rear long. Slips (λ_r)

In order to keep δ_1 within reasonable values, the steering amplitude is selected as the value that crosses the 2% band of the minimum time. This condition is expressed by (22):

$$\delta_1 = \delta(1.02 \min(t_{\alpha r})) \quad (22)$$

C. State 2 (Sideslip generation)

Once State 2 is initiated, the Algorithm 2 is activated.

Algorithm 2 Target rear slip detection

Input: Estimated rear slip ($\hat{\alpha}_r$)

Output: System State, Vehicle inputs ($\delta, \lambda_f, \lambda_r$)

1: If $abs(\hat{\alpha}_r)<abs(\alpha_{rref})$

2: $\delta = \delta_1, \lambda_f = 0, \lambda_r = -1$,

3: State=State 2

4: Else

5: $\delta = \delta_2 \cdot sign(M_{zref}), \lambda_f = 0, \lambda_r = 0$,

6: State=State 3

7: end

Where the rear wheel slip ($\hat{\alpha}_r$) is estimated from the expressions (23-24) and the steering input δ_2 is calculated using the kinematic relationship (25):

$$\hat{v}_y = \int (a_y - r v_x) \quad (23)$$

$$\hat{\alpha}_r = -\left(-\frac{r l_r}{v_x} + \frac{\hat{v}_y}{v_x}\right) \quad (24)$$

$$\delta_2 = SR \cdot \left(\alpha_{fref} + \frac{r l_f}{v_x} + \frac{\hat{v}_y}{v_x}\right) \quad (25)$$

D. State 3 (End of maneuver)

Finally, the Machine returns to State 1 when the time condition t_{end} is surpassed.

Algorithm 3 Return to initial state

Input: simulation time (t)

Output: System state

1: If $t < t_{end}$

2: $\delta = \delta_2, \lambda_f = 0, \lambda_r = 0$,

3: State=State 3

4: Else

5: $\delta = 0, \lambda_f = 0, \lambda_r = 0$,

6: State=State 1

7: end

VI. RESULTS

This section is intended to demonstrate the resemblance between the behavior of the *FSM* proposed in this paper and the Rally driving techniques employed when high yaw accelerations are required. In order to simplify the analysis, constant speed conditions are assumed, thus neglecting the effects of the rear wheel locking and induced drag in the longitudinal dynamics. Future works will consider these situations.

A. Target yaw Moment Sweep

First of all, several simulations were performed increasing the target yaw moment. In *"Fig. 15 a"* it can be seen how the machine starts switching to the intermediate State 2 when the target yaw moment is higher than 8KNm. *"Fig. 15 b"* illustrates the time histories of the yaw moment values obtained in the simulation.

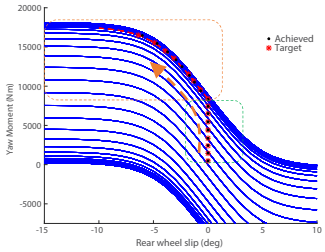

Fig. 15. a. Target yaw moment tracking.

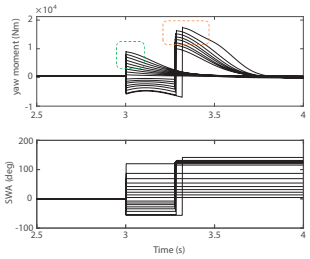

Fig. 15. b. Yaw moment and steering input time histories.

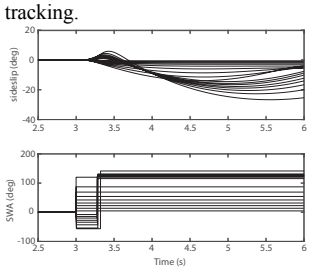

Fig. 16. a. Sideslip angle time histories.

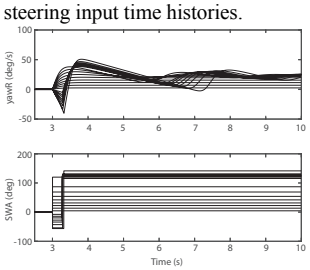

Fig. 16. b. Yaw rate time histories.

Sideslip and yaw rate time histories are presented in *"Fig. 16 a"* and *"Fig. 16 b"* respectively. Note how the sideslip increases considerably with the target yaw moment.

B. *Maximum yaw acceleration*

Now, consider the following common situation in Rally driving. The driver is about to negotiate a 90 deg left turn and he desires to rotate the vehicle quickly, in order to align its heading angle with the exit straight and go back to the throttle earlier, achieving higher exit speed [14]. Two scenarios are considered:

In the first situation, *"Fig. 17 a"*, the driver applies a step input and generates the maximum yaw moment derived from the front tires (only steering input).

In the second scenario, *"Fig. 17 b"*, the state machine applies the same steering input, but after going through State 2 (sideslip + steering input).

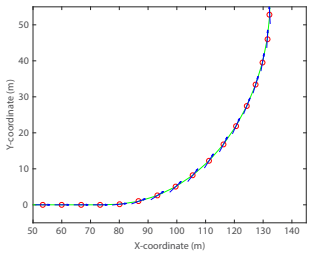

Fig. 17. a. Vehicle trajectory, normal Step.

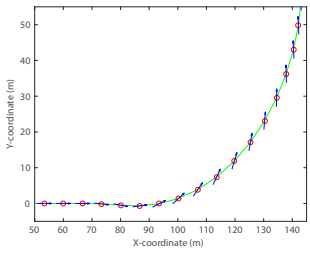

Fig. 17. b. Vehicle trajectory, max. yaw moment strategy.

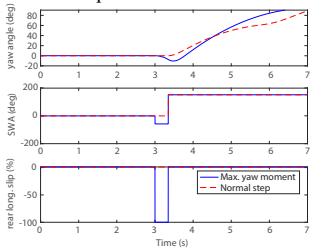

Fig. 18. a. Yaw angle, steering and long. slip time histories.

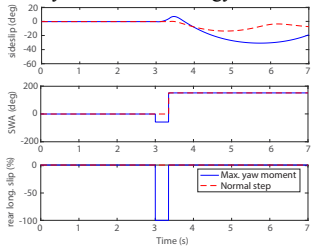

Fig. 18. b. Sideslip angle, steering and long. slip time histories.

As can be seen in *"Fig 18. a"*, the time to reach the 90 deg yaw condition is reduced (0.7s) when the max. yaw moment strategy is applied. Once the vehicle has been rotated, the driver can apply full throttle earlier and benefit from higher exit speed.

TABLE IV. Agility metrics

Notation	Normal Step strategy	Max yaw Acc. strategy	Unit
$\dot{r}_{max}$	197	384	$[°/s^2]$
$t_{\Psi 90}$	3.7	3.0	$[s]$
β_{min}	-13.4	-30.6	[°]
$\dot{\beta}_{min}$	-16.6	-35.5	[°/s]

Table. IV presents a comparison of the maximum yaw acceleration ($\dot{r}_{max}$), time to rotate the vehicle ($t_{\psi 90}$), minimum sideslip (β_{min}) and minimum sideslip rate ($\dot{\beta}_{min}$). Numerical values confirm that in order to maximize vehicle yaw acceleration and provoke high sideslip angles it is necessary to apply a high yaw moment strategy.

VII. CONCLUSIONS

In this paper, a new approach towards agile maneuvering has been proposed. Using widely recognized vehicle handling representations, it has been demonstrated that in order to maximize vehicle agility it is necessary to combine steering inputs with sideslip angles. This explains why Rally drivers excite the yaw dynamics when they approach hairpin turns in maneuvers such as the Scandinavian Flick.

Furthermore, an *FSM* has been developed to perform autonomously the inputs required to reach high agility regions. Results demonstrate that the sequence of inputs executed by the *FSM* resemble skilled driver actions when the vehicle attitude is to be rotated fast. The contribution of this paper is significant in what concerns *drift* generation and it is intended to integrate the *FSM* action with *drift* and *vehicle posture control* in further research steps.

Finally, extensive research in vehicle state estimation is being carried out in order to integrate these algorithms into a real vehicle and validate the results experimentally.

ACKNOWLEDGMENT

"This project has received funding from the European Union's Horizon 2020 research and innovation program under the Marie Skłodowska-Curie grant agreement No 675999"

REFERENCES

[1] W.F.Milliken, D.L.Milliken, "Race Car Vehicle Dynamics",SAE International, 1995.

[2] M.Blundell, D.Harty, "The Multibody Systems Approach to Vehicle Dynamics", ElSevier, 2014.

[3] S. Kanarachos, M. Blundell and A. Kanarachos, "Minimum vehicle slip path planning for automated driving using a direct element method", Proceedings of the Institution of Mechanical Engineers, Part D: Journal of Automobile Engineering, 2015.

[4] S. Kanarachos, M. Alirezaei, S. Jansen and J. Maurice, "Control allocation for regenerative braking of electric vehicles with an electric motor at the front axle using the state-dependent Riccati equation control technique", Proceedings of the Institution of Mechanical Engineers, Part D: Journal of Automobile Engineering, vol. 228, no. 2, pp. 129-143, 2013.

[5] A Zanten. "Evolution of electronic control systems for improving the vehicle dynamic behavior." *Proceedings of the 6th International Symposium on Advanced Vehicle Control*. 2002.

[6] Y. Shibahata, K. Shimada, T. Tomari, "Improvement of Vehicle Maneuverability by Direct Yaw Moment Control", in *Vehicle System Dynamics*, 22 (1993), pp. 465 – 481.

[7] E. Velenis, P. Tsiotras and J. Lu, "Modeling aggressive maneuvers on loose surfaces: The cases of Trail-Braking and Pendulum-Turn," *Control Conference (ECC), 2007 European*, Kos, 2007, pp. 1233-1240.

[8] B. Olofsson, K. Lundhal, K. Berntorp, L. Nielsen, "An investigation of optimal vehicle maneuvers for different road conditions", *7th IFAC Symposium on Advances in Automotive Control, 2013*.

[9] J. Edelmann, M. Plöchl, "Handling characteristics and stability of the steady-state powerslide motion of an automobile", *Regular and Chaotic Dynamics*, Vol. 14, No. 6. (1 December 2009), pp. 682-692.

[10] E. Velenis, D. Katzourakis, E. Frazzoli, P. Tsiotras, R. Happee, "Steady-state drifting stabilization of RWD vehicles", *Control Engineering Practice*, Vol. 19, Issue 11, November 2011, pp 1363-1376.

[11] J. Li, Y. Zhang, J. Yi, Z.Liu, "Understanding Agile Maneuver Driving Strategies Using Coupled Longitudinal / Lateral Vehicle Dynamics", *ASME 2011 Dynamic Systems and Control Conference.* 2011.

[12] D. Kang, J.L. Stein, R.C. Hoffman, L.S. Louca, K. Huh, "Implementing the Milliken Moment Method using Controlled Dynamic Simulation", *SAE Vehicle Dynamics and Simulation*, 2005, pp 93 – 100.

[13] R.C. Hoffman, J.L. Stein, R.C. Hoffman, L.S. Louca, K. Huh, "Using the Milliken Moment Method and Dynamic simulation to evaluate Vehicle Stability and controllability", *International Journal of Vehicle Design (IJVD)*, Vol. 48, No. 1/2, 2008.

[14] M.White, Measurement and Analysis of Rally Car Dynamics at High Attitude Angles, Ph.D. Thesis, Cranfield University.

NOMENCLATURE

$\boldsymbol{N}$:	Yaw moment
$\boldsymbol{C_N}$:	Normalized Yaw moment
$\boldsymbol{m}$:	Vehicle mass
$\boldsymbol{g}$:	Gravity
$\boldsymbol{l_f}$:	Front axle distance to centre of gravity
$\boldsymbol{l_r}$:	Rear axle distance to centre of gravity
$\boldsymbol{t_{wf}}$:	Front track width
$\boldsymbol{t_{wr}}$:	Rear track width
$\boldsymbol{I_z}$:	Yaw inertia
$\boldsymbol{k_{\varphi f}}$:	Front roll stiffness
$\boldsymbol{k_{\varphi r}}$:	Rear roll stiffness
$\boldsymbol{h_{CoG}}$:	Centre of gravity height
$\boldsymbol{SR}$:	Steering ratio
$\boldsymbol{F_{xi}}$:	Tire longitudinal force
$\boldsymbol{F_{yi}}$:	Tire lateral force
$\boldsymbol{\delta}$:	Steering angle
$\boldsymbol{v_x}$:	Vehicle longitudinal speed
$\boldsymbol{v_y}$:	Vehicle lateral speed
$\boldsymbol{r}$:	Yaw rate
$\boldsymbol{\alpha_i}$:	Wheel slip
$\boldsymbol{\alpha_{f,r}}$:	Linearized wheel slip
$\boldsymbol{WB}$:	Wheel base
$\boldsymbol{\Delta F_{z,long}}$:	Longitudinal weight transfer
$\boldsymbol{\Delta F_{z,lat}}$:	Lateral weight transfer
$\boldsymbol{\beta}$:	Sideslip angle
$\boldsymbol{\alpha_{rref}}$:	Rear reference wheel slip (maneuverability map)
$\boldsymbol{\alpha_{fref}}$:	Front reference wheel slip (maneuverability map)
$\boldsymbol{\lambda_{f,r}}$:	Longitudinal wheel slip
$\boldsymbol{M_{zref}}$:	Reference yaw moment (maneuverability map)
$\boldsymbol{M_{z1}}$:	Yaw moment threshold
$\boldsymbol{\hat{\alpha}_r}$:	Estimated rear wheel slip
$\boldsymbol{\hat{v}_y}$:	Estimated lateral velocity
$\boldsymbol{\delta_1}$:	First steering input (maneuverability map)
$\boldsymbol{\delta_2}$:	Second steering input (maneuverability map)
$\boldsymbol{t_{5r}}$:	Time to reach a rear wheel slip angle of 5 degrees
$\boldsymbol{t_{10r}}$:	Time to reach a rear wheel slip angle of 10 degrees
$\boldsymbol{t_{15r}}$:	Time to reach a rear wheel slip angle of 15 degrees
$\boldsymbol{\dot{r}_{max}}$:	Maximum yaw acceleration
$\boldsymbol{t_{\psi 90}}$:	90 degrees heading rotation time
$\boldsymbol{\beta_{min}}$:	Minimum sideslip value
$\boldsymbol{\dot{\beta}_{min}}$:	Minimum sideslip rate value